Applied Catalysis B: Environmental 219 (2017) 344–352

Contents lists available at ScienceDirect

Applied Catalysis B: Environmental

journal homepage: www.elsevier.com/locate/apcatb

Surface modification of TiO_2 nanoparticles by magnetic ions: Synthesis and application in enhancement of photocatalytic performance

Mansoor Farbod*, Marzieh Kajbafvala

Physics Department, Faculty of science, Shahid Chamran University of Ahvaz, Ahvaz, Islamic Republic of Iran

ARTICLE INFO

Article history:
Received 15 April 2017
Received in revised form 30 June 2017
Accepted 21 July 2017
Available online 24 July 2017

Keywords:
Gd doped TiO_2
Sm doped TiO_2
Combined sol–gel milling method
Nanocomposite
Photocatalysis

ABSTRACT

The surface of TiO_2 nanoparticles was modified by Samarium (Sm) and Gadolinium (Gd) doping to enhance their adsorption and photocatalytic performance. The undoped TiO_2 and different (Sm or Gd)/Ti molar ratios of 0.9, 1.8 and 3.6 at.%, were prepared through a combined sol-gel milling method and sintered in two different temperatures of 550 and 700 °C. Scanning electron microscope (SEM) images of composite samples revealed a clear reduction in particle size compared to the undoped samples of the same temperature. Excellent adsorption and photodegradation of Congo red dye solution under ultraviolet (UV) irradiation were attained for Sm-TiO_2 and Gd-TiO_2 nanoparticles compared to the undoped samples sintered at the same temperature. The photocatalytic performance of composites was improved up to 1.8 at.% of Sm or Gd content. The results showed that the Gd-TiO_2 composite nanoparticles had much better performance compared to the Sm-TiO_2 composite nanoparticles with the same molar ratio and the same sintering temperature.

1. Introduction

Photocatalysis is a surface phenomenon that plays an important role in pharmaceutical, petrochemical, chemical and wastewater treatment industries especially in gas and oil fields. Photocatalytic properties of materials are not only materials-dependent, but also exceptionally are shape and size dependent; therefore, photocatalyst nanomaterials can exhibit very different behavior as compared to their bulk counterpart [1].

Titanium dioxide is the most common functional material in the photocatalyst semiconductors but unfortunately suffers from narrow light response range and so low efficiency [2,3]. The other reason for low efficiency of photocatalytic property of TiO_2 is its very fast recombination of electron-hole pairs which are produced with light absorbance [4–7]. It has been investigated that the nanocomposites of titanium dioxide and some transition metallic elements such as Fe, Ni, V, Cr, Co and Zn [5–8] or some nonmetallic elements such as S, F, Cl, Br, I, N [9–12] and C in its varied forms including carbon nanotubes (CNTs), fullerenes and graphene [13–17] are able to reveal enhanced photocatalytic performance compared to the pure TiO_2. Furthermore, the effect of TiO_2 doping with some noble metals such as Au, Pt and Ag [18–20], and some alkaline earth metal ions such as Mg, Be, Ca and Sr [21] on its photocatalytic activity had previously been studied. Also, the doping effect of some metals such as Al, Ga, In, Sn and Pb [22,23] and metalloids such as Si, Ge and B [24] on the enhancement of TiO_2 photocatalytic performance has been investigated and no significant improvement has been observed.

Finally, some attention has been also paid to the rare earth metals due to their unique properties [25–28]. These elements have incomplete occupied 4f and empty 5d orbitals often used as catalysts or improved catalytic properties due to the transition of 4f electrons in their ions, which led to an improved optical adsorption of the photocatalysts and reinforced the separation of photo generated electron-hole pairs [29–32]. Furthermore, the incorporation of rare earth metal ions into the TiO_2 matrix could increase the adsorption of organic pollutants at the semiconductor surface, hence promoting the photoactivity of TiO_2 [33,34]. Some good reviews have been published about the rare earth doping of TiO_2 [35,36]. Many effects of such doping have been discussed ranging from the effect of rare earths during sintering which can affect the structure, purity, morphology and other qualities of TiO_2 to the effect of rare earth ions doped only on the photocatalytic performance of TiO_2 which are related to the f electrons of rare earth. The mechanisms for these effects proposed by different researchers have not been the same and in some cases some opposite inter-

* Corresponding author.
E-mail address: farbod_m@scu.ac.ir (M. Farbod).

http://dx.doi.org/10.1016/j.apcatb.2017.07.060
0926-3373/

pretations have been proposed. Therefore it seems more studies needed to elucidate the mechanisms governed by all these various effects.

In present study, TiO_2 nanopowders without and with gadolinium (Gd) and samarium (Sm) ion dopants were prepared through the combined sol-gel milling method. For both composite samples the molar ratios of dopants were 0.9, 1.8 and 3.6 at.%. Also, two sets of each nanocomposite were prepared by sintering the initial materials at 550 and 700 °C, separately. Photocatalytic degradation of Congo red dye was investigated after dark experiment for the all prepared samples as photocatalyst.

2. Experimental

2.1. Photocatalysts synthesis

All reagents, including titanium tetra-isopropoxide (TTIP, Merck, Germany), absolute ethanol (Merck, Germany), ammonia (25%, Merck, Germany), Gadolinium (III) nitrate hexahydrate (99.90% pure grade, Acros, New Jersey, USA), and Samarium (III) nitrate hexahydrate (99.90% pure grade, Alfa Aesar, Germany) were used as received.

Undoped TiO_2, Sm-TiO_2 and Gd-TiO_2 composite nanopowders were prepared using a combined sol–gel milling process explained in details in our previous work [25]. In this method, hydrolysis begins by adding de-ionized water to TTIP dissolved in absolute ethanol. Then, Gd (III) nitrate hexahydrate or Sm (III) nitrate hexahydrate, as sources of lanthanide ions, dissolved in absolute ethanol was added drop wised to the initial solution. The pH was maintained at 9 by addition of ammonia during the process. The solvent was evaporated at 50 °C, washed with de-ionized water, kept overnight at room temperature and then dried by oven at 115 °C. The undoped samples were synthesized by the same method without adding dopant source. In the last step before sintering, the products were milled using a planetary ball mill with a speed of 500 rpm for 30 min. At last, all resulting amorphous powders were sintered at 550 and 700 °C, separately. The molar ratios of TTIP, absolute ethanol and de-ionized water were selected as 1:10.66:33.34, respectively. The Sm and Gd doped samples were prepared with the molar ratios of (Sm or Gd): Ti as: 0.9, 1.8 and 3.6.

2.2. Sample's characterization

The crystalline structure of the samples was determined by X-ray diffraction (XRD) using a Philips, PW1840 diffractometer at room temperature utilizing Cu Kα radiation wavelength of λ = 1.5418 Å. The peak position and intensities were obtained between 10 and 80° with a velocity of 0.02° per second. A field emission scanning electron microscope (Hitachi, S4160) was used to determine the particle size and morphology of the samples. The Brunauer-Emmett-Teller (BET) specific surface area, barrett-Joyner-Halenda (BJH) pore size distribution plots and N_2 adsorption-desorption isotherms were measured on BELSORP-mini II (Japan) to further study of microstructure of the samples. UV–vis absorption measurement was done by use of a GBC, Cintra 101 spectrophotometer. The photoluminescence (PL) spectra were recorded with LUMINA fluorescence spectrometer at an excitation wavelength of 335 nm. The photoelectrochemical measurements (photocurrent and electrochemical impedance spectroscopy (EIS)) were carried out on a three electrode electrochemical workstation using an electrochemical analyzer (Autolab PGSTAT302N) equipped with a solar simulator (LCS-100^{TM}, 100W Ozone-free Xenon lamp).

2.3. Photocatalytic activity and adsorption measurements

The photocatalytic activity of the prepared nanoparticles was determined by measuring the degradation rate of Congo red dye solution using a home-made photoreactor with two 15 W ultraviolet (UV) lamps which were used as the irradiation UV source [25]. For this purpose, 100 mL of the dye solution (20 mg/L) and 0.1 g photocatalyst nanopowder were placed in a glass beaker. In each experiment, prior to UV irradiation, the colloidal solution stirred in the dark for 60 min (as a reference point). The solution was then irradiated under UV light for 210 min. The sampling was done every 30 min in order to measure the dye concentration. The change in concentration of centrifuged solution was determined using the UV–vis spectrophotometer. The absorptivity measurements were carried out at wavelength range of 400–700 nm, because the maximum light absorption by the dye occurs at this wavelength range. All of these experiments were done at room temperature. The micro mechanisms of the dark and photocatalytic experiments were explained in details at our previous work [25].

2.4. Photoelectrochemical measurements

Photoelectrochemical measurements of the prepared samples were carried out on a three electrode electrochemical workstation equipped with a platinum wire as the counter electrode, an Ag. AgCl/3 M KCl electrode as the reference electrode and a fluorine-doped tin oxide (FTO) coated with prepared samples as the working electrode. All experiments were carried out in 100 mL of 0.05 molar Na_2SO_4 aqueous solutions as electrolyte without bias potential under simulated solar light irradiation at room temperature. The reaction vessel was placed about 25 cm away from the lamp. For preparing the working electrodes, 0.3 mL of 50 gL^{-1} dense dispersions of corresponding synthesized samples were dropped casted on $1 \times 1.5\ cm^2$ FTO followed by drying at 70 °C in an oven. The prepared coated FTOs then annealed at 500 °C for an hour. At the end, a $1 \times 1\ cm^2$ specific surface area of coated FTOs induced to electrolyte for measurements. In order to stabilize the photocurrent, each of working electrodes was light irradiated for 400 s prior to starting the photocurrent measurements, then the current was measured in 50 s intervals of on and off lamp. The charge transfer resistance was determined by EIS measurements at open circuit potential under similar conditions as described above for photocurrent tests and under simulated solar light irradiation. The amplitude and the frequency range of EIS tests set as 10 mV and 100 kHz-0.01 Hz, respectively.

3. Results and discussion

3.1. XRD analysis

Fig. 1 compares the XRD patterns of undoped TiO_2 nanopowder, Sm-TiO_2 composite nanopowder and Gd-TiO_2 composite nanopowder both in molar ratios of 0.9, 1.8 and 3.6 that all of them have sintered at 700 °C. The undoped sample sintered at 700 °C is a combination of both anatase and rutile phases with the main anatase peak at $2\theta = 25.31°$ according to the JCPDS card number of 73-1764 and a short main rutile peak at $2\theta = 27.94°$ (JCPDS-84-1284).

Fig. 1 confirms that all of the doped samples sintered at 700 °C are pure anatase phase with diffraction patterns which are matched with that of the undoped TiO_2 sintered at the same temperature except for the existence of a tiny rutile phase peak. It means that for doped samples, the corresponding short and emerged rutile peak disappears completely after sintering at 700 °C. To the best of our knowledge, such high temperature anatase stability has not been

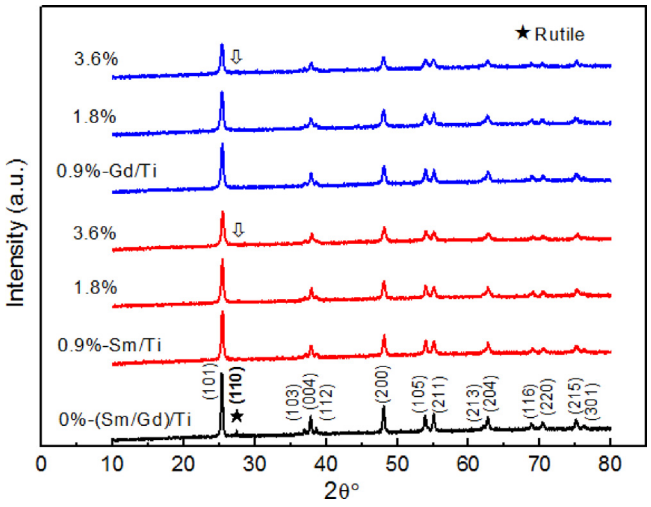

Fig. 1. XRD patterns of undoped TiO_2, 0.9, 1.8 and 3.6 at.% Sm-TiO_2 nanocomposites and 0.9, 1.8 and 3.6 at.% Gd-TiO_2 nanocomposites sintered at 700 °C.

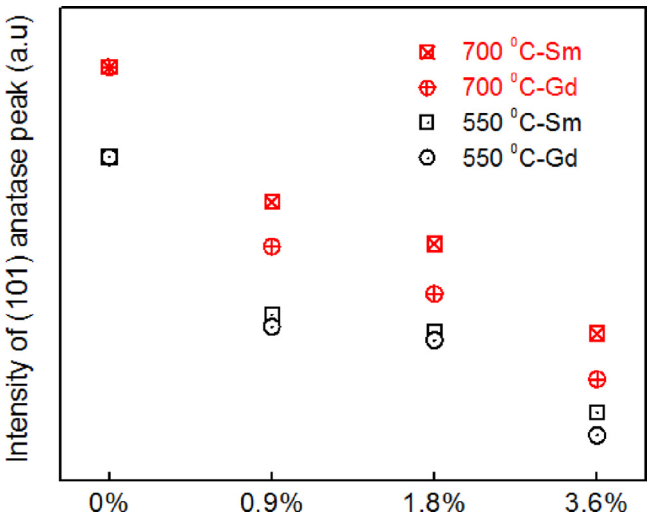

Fig. 2. Intensity of (101) anatase peak of x-ray diffraction analysis for 0, 0.9, 1.8 and 3.6 at.% Sm-TiO_2 and Gd-TiO_2 nanocomposites sintered at 550 and 700 °C.

reported so far. In fact the presence of rare earth dopant at the interstitial sites can hinder the ionic mobility which is needed to anatase-rutile phase transition and so affects the grain growth rate and the density of rutile nucleation. In addition, the absence of any peak related to the dopant in Fig. 1 could be due to the uniformly distributed of Sm and Gd ions in the interstitials sites. Indeed, it is because of the ionic radius of Sm or Gd ions which are much larger than that of Ti, so these cations can't substitute at the Ti sites in the TiO_2 lattice. This can cause a distortion in the TiO_2 lattice and its crystallinity is decreased when the doping is high. Observed uniform decrease of diffraction peaks in the doped samples with increasing the amount of dopant in Fig. 1 confirms such gradual descent in crystallinity. Comparison of diffraction patterns of doped and undoped samples in Fig. 1 also confirms that no displacement of the peaks occurs which is a sign of lack of substitution of lanthanide ions into the TiO_2 lattice.

It should be noted that the all undoped and composite samples which were sintered at 550 °C, were crystallized in pure anatase phase with the main peak at $2\theta = 25.31°$ according to the JCPDS card number of 73-1764. Also the color of all samples was white.

Fig. 2 shows intensity of (101) anatase peak for 0, 0.9, 1.8 and 3.6 at.% molar ratios of Sm-TiO_2 and Gd-TiO_2 sintered at 550 and 700 °C, respectively. As represented in Fig. 2, by increasing the sintering temperature the lattice crystallinity improves, therefore all

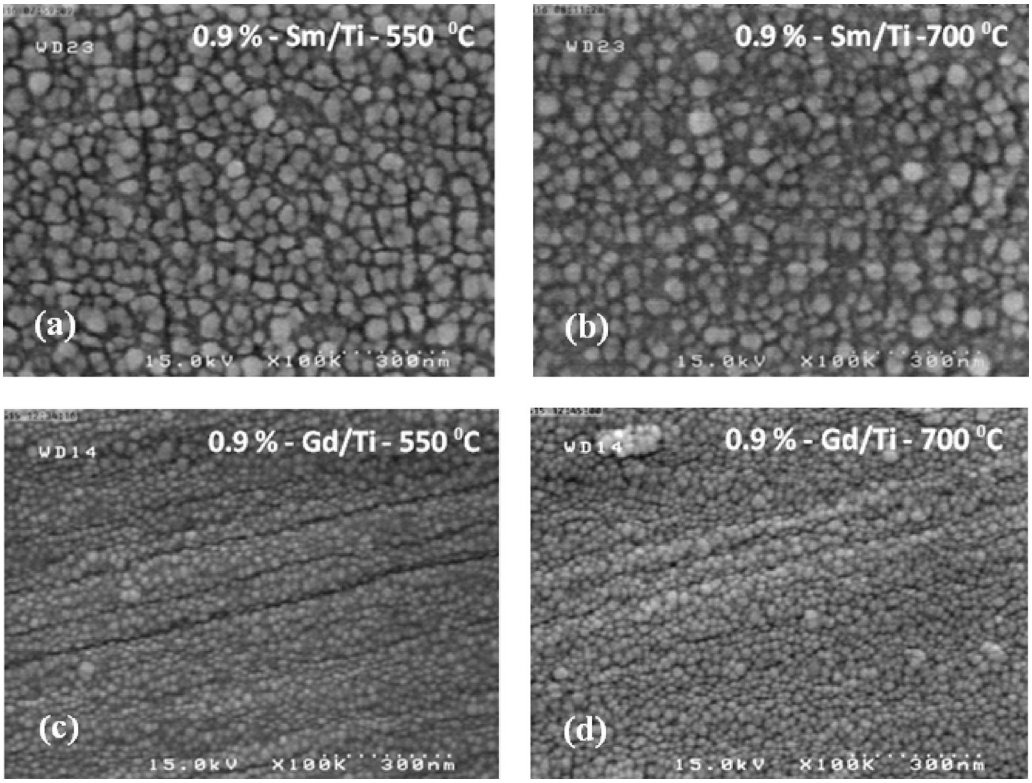

Fig. 3. SEM images of 0.9 at.%-Sm-TiO_2 nanocomposite sintered at (a) 550 °C and (b) 700 °C and SEM images of 0.9 at.%-Gd-TiO_2 nanocomposite sintered at (c) 550 °C and (d) 700 °C.

Table 1
BET and Langmuir data of the samples sintered at 700 °C.

Sample	BET surface area (m^2/g)	Langmuir surface area (m^2/g)
Pure TiO_2	5.655	59.7
0.9 at.%-Sm/TiO_2	9.763	164.7
0.9 at.%-Gd/TiO_2	22.951	282.2

the samples sintered at 700 °C had more crystallinity than the samples sintered at 550 °C. Also, Gd ions in all samples were more effective than Sm ions in reduction of lattice crystallinity in both sintering temperatures. Furthermore, by increasing the molar ratio of Sm or Gd ions, the lattice crystallinity was further reduced.

3.2. SEM and BET analysis

Fig. 3a and b represent SEM images of 0.9 at.% of Sm-TiO_2 nanocomposites sintered at 550 and 700 °C, respectively. Also, Fig. 3c and d show the SEM images of 0.9 at.% Gd-TiO_2 nanocomposites sintered at 550 and 700 °C, respectively. All figures show the nanoparticles have a spherical shape. Comparison of Fig. 3a and b for 0.9 at.% of Sm-TiO_2 nanocomposites sintered at 550 and 700 °C and Fig. 3c and d for those of Gd dopant show that the sintering temperature has no effective influence on the size of nanoparticles. It should be mentioned that the particle size of all composite nanoparticles were smaller compared to that of the undoped samples. This procedure has been observed for both composite nanoparticles with Sm and Gd sintered at two different temperatures of 550 and 700 °C.

Using the SEM images, the size of about 100 nanoparticles was measured by an SEM image analyzer called Digimizer and their average was reported. The error in measuring the particles' size was about ±3 nm. The average particle size of Sm-TiO_2 nanocomposites and of Gd-TiO_2 nanocomposites were in the range of (19–24) ±3 nm and of (12–15) ±3 nm, respectively. So, the Gd-TiO_2 nanoparticles were smaller than the Sm-TiO_2 nanoparticles, maybe because the ionic radius of Gd ions is smaller than the ionic radius of Sm ions. Finally, the comparison of Fig. 3a and b corresponded to the Sm-TiO_2 nanocomposites and Fig. 3c and d corresponded to the Gd-TiO_2 nanocomposites revealed that the Gd-TiO_2 nanocomposites have more uniform size distribution than the Sm-TiO_2 nanocomposites.

Table 1 lists the BET and Langmuir surface area data for undoped and 0.9 at.% of Gd- and Sm-doped samples sintered at 700 °C. One can observe from the table that the Gd-doped sample shows a bigger surface area (22.951 m^2/g) in comparison with the Sm-doped sample (9.7628 m^2/g) and the undoped one (5.6547 m^2/g). These results are compatible with the SEM images (Fig. 3) that the particle sizes of the Gd-doped samples were very smaller than that of the Sm-doped and undoped samples and so the surface area must be larger.

Fig. 4a and b show the adsorption-desorption isotherms and Barrett-Joyner-Halenda (BJH) pore size distribution plots of undoped TiO_2, 0.9 at.% Sm and 0.9 at.% Gd doped TiO_2 samples sintered at 700 °C respectively. It is to be mentioned that the Langmuir surface area is the maximum limit of adsorption so is bigger than the BET surface area. It is clear from Fig. 4a that the isotherm curves of the samples exhibit a typical irreversible adsorption-desorption behavior due to the presence of the pores and confirms that the Gd-doped TiO_2 has much more pores compared to the other two samples. The corresponding BJH pore size distribution plots (Fig. 4b) also confirm that the Gd-doped TiO_2 samples have more porosity compared to the Sm-doped and the undoped samples. Having porous structure has very effective impacts on the properties of a sample such as photocatalytic and photocurrent for which the larger the specific surface area the better performance would be. The higher porosity of the Gd-doped samples causes a better

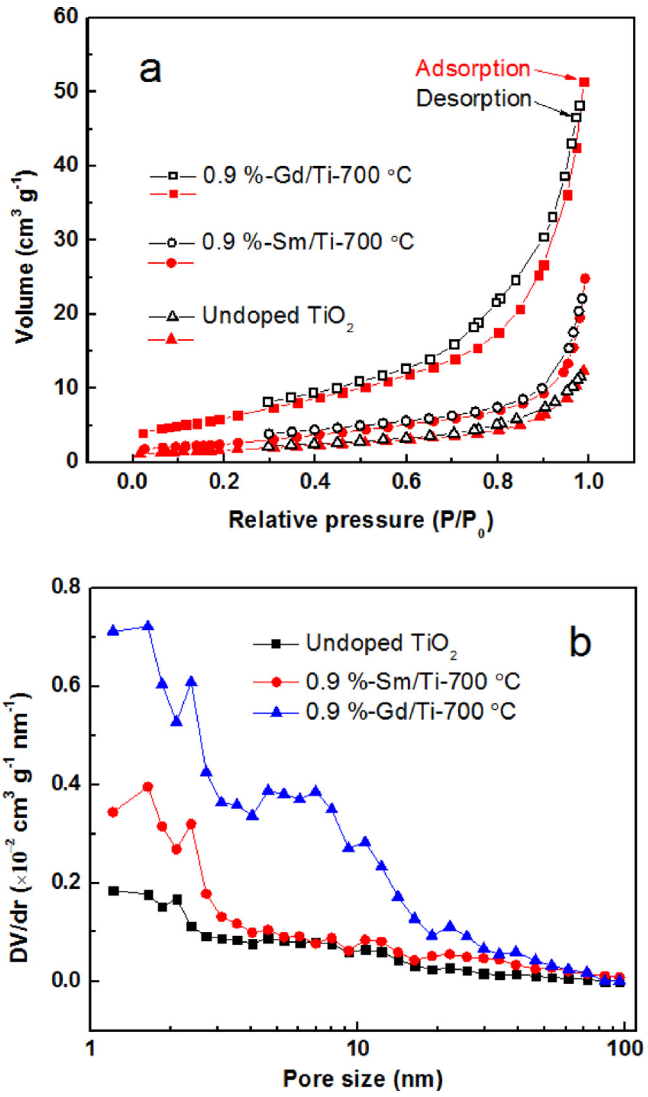

Fig. 4. N_2 adsorption/desorption isotherm curves (a) and BJH pore size distribution of undoped TiO_2, 0.9 at.%-Sm-TiO_2 and 0.9 at.%-Gd-TiO_2 sintered at 700 °C (b).

diffusion of light into the sample's nanoparticles and can increase their photocatalytic performance. Also, this property can increase the contact surface between the working electrode and electrolyte and therefore decrease the charge transfer resistance resulting in the photocurrent enhancement of the Gd-doped samples (Fig. 9).

3.3. Photoluminescence measurements

The photoluminescence (PL) spectra of the prepared samples were recorded at an excitation wavelength of 335 nm. Fig. 5a and b shows the PL spectrum of undoped, Sm- and Gd-doped TiO_2 samples sintered at 700 °C. One can observed that (inset of Fig. 5a) the intensity of PL emission bands for Gd-doped samples is very smaller than corresponding Sm-doped ones, suggesting a fast photoinduced electron transfer for Gd-TiO_2 nanocomposites which leads to decreasing the recombination rate of photogenerated electron-hole pairs and reaching them to the surface [37,38]. In contrast, having the higher PL intensity of Sm-TiO_2 nanocomposites rather than Gd-TiO_2 nanocomposites (inset of Fig. 5a) means more recombination rate and thus less photoinduced carriers on the surfaces of Sm-doped TiO_2 particles.

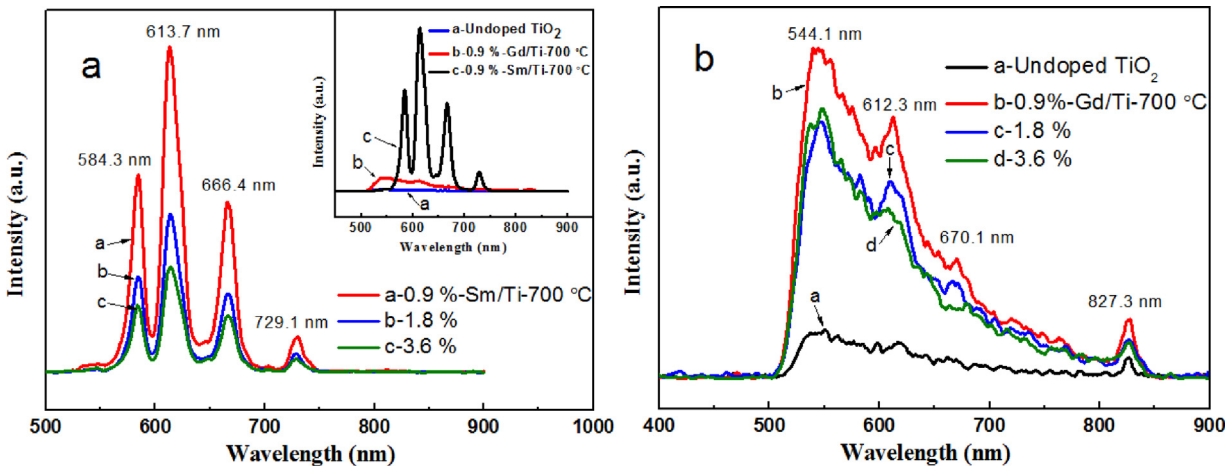

Fig. 5. PL spectra of 0.9, 1.8 and 3.6 at.% of Sm-TiO_2 nanocomposite sintered at 700 °C (a). The inset shows the comparison of PL spectra for undoped TiO_2, 0.9 at.% Sm-TiO_2 and 0.9 at.% Gd-TiO_2 sintered at 700 °C and PL spectra of undoped, 0.9, 1.8, 3.6 at.% Gd-TiO_2 nanocomposite sintered at 700 °C (b).

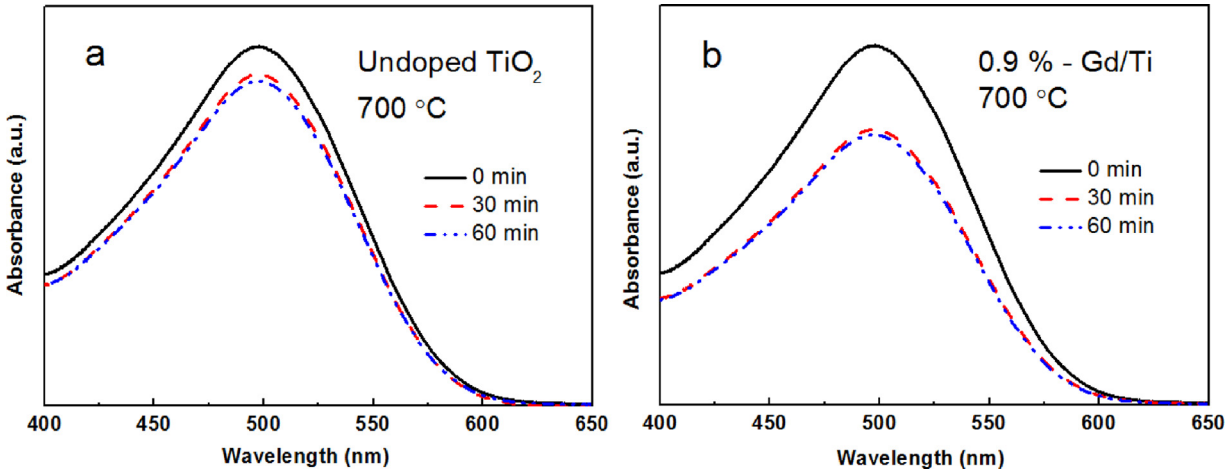

Fig. 6. UV–vis spectra of Congo red solutions after 0, 30 and 60 min dark experiment in presence of (a) undoped TiO_2 nanoparticles, (b) 0.9 at% Gd-TiO_2 composite nanoparticles sintered at 700 °C.

3.4. Dark experiments and photocatalytic activity results

As mentioned in Section 2.3, the dark experiment was performed for all prepared samples in aqueous solution of Congo red prior to direct illumination of UV light for 60 min. The UV–vis spectra of Congo red solutions after 0, 30 and 60 min dark experiment in presence of undoped TiO_2 nanoparticles and 0.9 at.% Gd-TiO_2 composite nanoparticles sintered at 700 °C have been represented in Fig. 6a and b respectively. It can be observed that dye adsorption of doped samples is higher than that of the pure samples. Also the dye adsorption has saturated after 30 min stirring of the solution in the dark.

Fig. 7 represents scatter graph of average particle size data and bar graph of dye adsorption percentage data after dark experiments for 0, 0.9, 1.8 and 3.6 at% Sm-TiO_2 and Gd-TiO_2 nanocomposite samples. Dye adsorption Percentages were calculated via equation $\frac{C_{CR}-C}{C_{CR}} \times 100$ where C_{CR} is the adsorption coefficient corresponds to the initial cocentration of the dye and C is the adsorption coefficient corresponds to the dye concentration after the dark experiment.

The represented results of Fig. 7 state that the adsorption increases by doping in comparison with the adsorption of undoped samples. So, both the Sm and Gd ions should play an important role in the adsorption procedure, because Congo red which is an anionic dye is adsorbed due to the positive electric charge of these surface ions. Moreover, it can be observed that the Sm-TiO_2 nanocomposites have adsorbed Congo red more than Gd-TiO_2 nanocomposites with the same molar ratio despite the former has larger particles and then lesser specific surface area. It may be due to the larger ionic radius of the Sm ions compared to that of the Gd ions which may produce further surface defects in Sm-TiO_2 nanocomposites and then increases the adsorption.

Also, it was found that by increasing the molar ratio of lanthanide ions, the adsorption was increased for all corresponding samples. This could be due to the increase in specific surface area which occurs with decreasing the size of the particles and therefore the surface density of positively charged lanthanide ions have been increased.

Finally, as Fig. 7 shows, the adsorption of the samples sintered at 550 °C is more than the adsorption of the same samples sintered at 700 °C for the same molar ratios, although their particle size was observed almost the same. As mentioned in Section 3.2, the composites with the same molar ratios of dopant (Sm or Gd) sintered at 550 and 700 °C had the same particle size and therefore the same specific surface area. So another reason should be responsible for the better adsorption of particles sintered at 550 °C. According to Fig. 2, the crystallinity of the samples with the same molar ratio and the same dopant sintered at 700 °C was increased compared to the corresponding samples sintered at 550 °C, so such increased crystallinity probably caused a reduction in surface defects resulting in

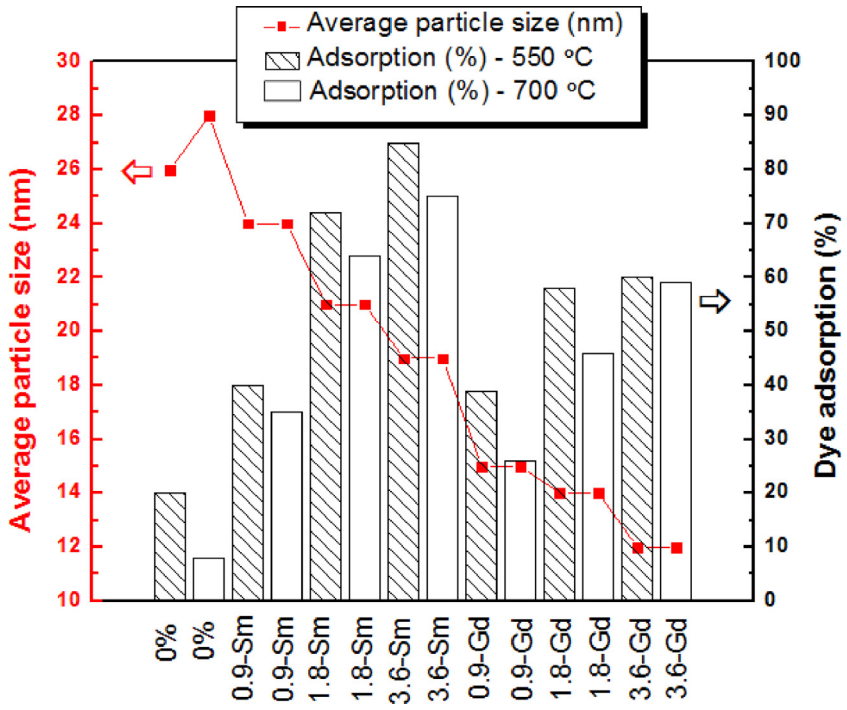

Fig. 7. Scatter graph of average particle size (left axis) and dye adsorption percentage of undoped, 0.9, 1.8 and 3.6 at.% Sm-TiO_2 and Gd-TiO_2 composite nanoparticles (right axis) sintered at 550 °C (dashed columns) and at 700 °C (blank columns).

a decrease in dye adsorption. But for undoped nanoparticles, dye adsorption of the samples sintered at 550 °C is higher than that of the samples sintered at 700 °C probably due to the smaller particle size of the sample sintered at 550 °C and therefore having bigger specific surface area. Also it was shown in Fig. 2 that the crystallinity of the samples sintered at 700 °C was higher and therefore the surface defects are less in comparison with the samples sintered at 550 °C which caused the adsorption reduction. Such a higher crystallinity which causes a reduction in surface defects can reduce the probability of the electron-hole recombination process which causes an increase in the photocatalytic performance.

Fig. 8 shows the normalized concentration of Congo red versus UV irradiation time in 30 min intervals in absence of photocatalyst and in presence of 0, 0.9, 1.8 and 3.6 at.% of Sm-TiO_2 and Gd-TiO_2 composite nanoparticles sintered at 550 and 700 °C, respectively.

From Fig. 8 it is clear that the dye degradation is higher in presence of doped samples which indicates the crucial role of the lanthanide ions in inhibition of electron-hole pair recombination.

Also according to Fig. 8a and b, all of the Gd-TiO_2 nanocomposite samples degrade the dye better than the Sm-TiO_2 samples with the same molar ratio and the same sintering temperature. As stated in Section 3.2, Gd doped samples had smaller particle size and so higher specific surface area resulting in their better photocatalytic performance. Furthermore, it can be observed by increasing the amount of dopants (Sm or Gd) from 0 to 1.8 at.% the photocatalytic performance increases but by further increase of dopants from 1.8 to 3.6 at.% the photocatalytic performance decreases. This procedure was observed for all samples sintered at both 550 and 700 °C. So one can deduce that the 1.8 at.% of dopant is an optimum amount. In fact by increasing the amount of dopant, the nanoparticle sizes decrease (Fig. 7) and the effective surface areas increase by which the surface defects and surface recombination of electron hole increases and reduces the photocatalytic performance of the samples.

From Fig. 8a one can observe that in the first hour of UV irradiation, the dye degradation by undoped TiO_2 is 42%. This ratio is 56, 70 and 56% for Sm-TiO_2 composite nanoparticles with 0.9, 1.8 and 3.6 at.% molar ratios respectively and is about 60, 76 and 74% of initial dye for Gd-TiO_2 nanocomposites with the same molar ratios respectively. The photocatalytic results are different when the samples are sintered at 700 °C. As can be observed from Fig. 8b after one hour UV irradiation, the dye degradation is just 35% for undoped TiO_2. The dye degradation is 63, 74 and 66% for Sm-TiO_2 nanoparticles with 0.9, 1.8 and 3.6 at.% molar ratios respectively and is about 71, 84 and 69% of initial dye for Gd-TiO_2 nanoparticles with the same molar ratios respectively. It is obvious that the photocatalytic performance of the samples sintered at 700 °C is much higher. The reason could be due to better crystallinity of the samples sintered at 700 °C so they can inhibit the electron-hole recombination better. Fig. 8c shows the reaction rate constant (k) of the samples which shows that among the all samples, the 1.8 at.% of Gd-doped samples which were sintered at 700 °C have higher photocatalytic performance. For testing the photocatalytic stability, cyclic degradation tests of Congo red dye were performed under the same conditions. After testing three repeated runs, the Congo red degradation was the same, indicating that the Gd-TiO_2 nanocomposites' performance is stable and can be used frequently.

3.5. Photoelectrochemical discussions and results

The photocurrent experiments can be used to investigate the ability of producing charge carriers and the separation efficiency of photogenerated electron-hole pairs [37–41]. The photocurrent of undoped TiO_2, Sm- and Gd-doped samples sintered at 700 °C are shown in Fig. 9a and b. From the figures one can observe that the TiO_2 nanocomposite samples response to the light, much better than the undoped TiO_2 and their intensity of the photocurrent shows a significant increase compared to the undoped one. Also the Gd-doped samples show much stronger photocurrent intensity (Fig. 9b) in comparison with the corresponding Sm-doped ones (Fig. 9a). This means that the Gd-doped samples have stronger ability to produce charge carriers so more electrons and holes could be transferred to the surface of particles and participate in the photocatalytic reactions. Additionally, one can observe that

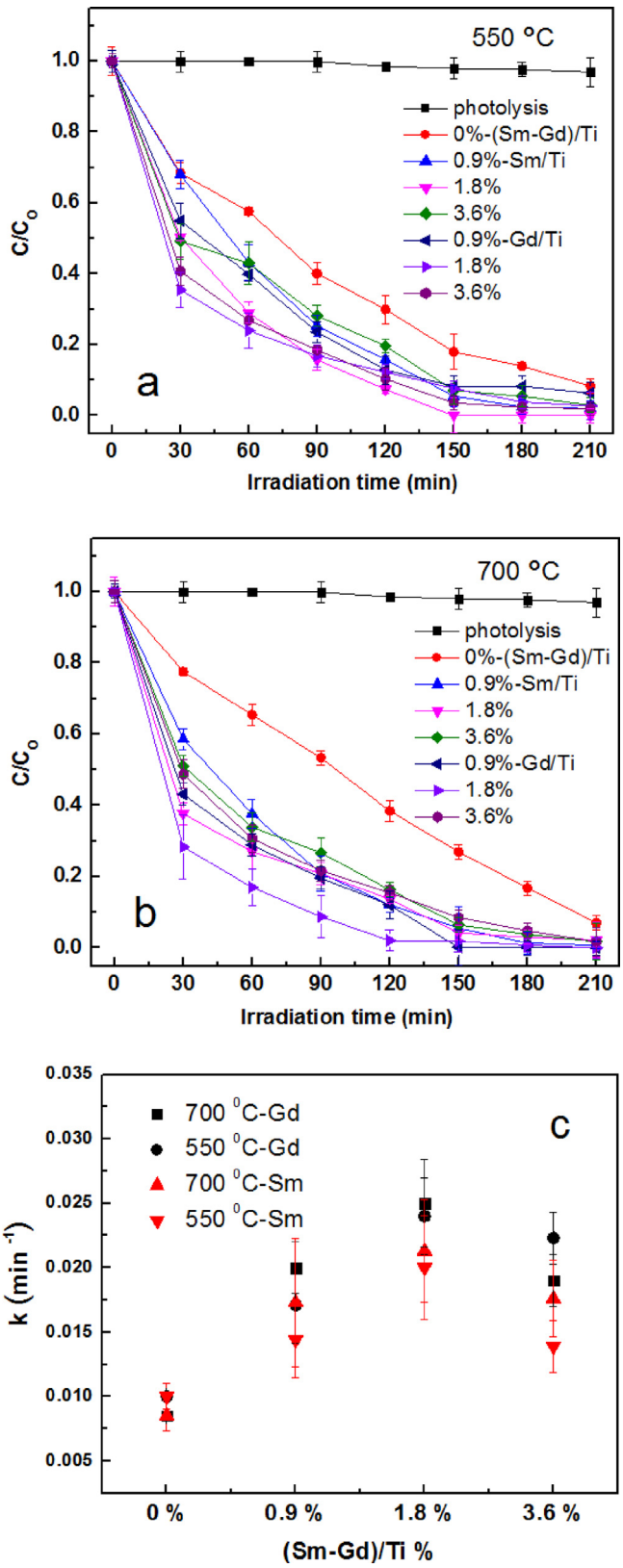

Fig. 8. Normalized concentrations of Congo red dye versus UV irradiation time in absence of photocatalyst (photolysis) and in presence of undoped, 0.9, 1.8 and 3.6 at.% Sm-TiO_2 and Gd-TiO_2 composite nanoparticles sintered at (a) 550 °C and (b) 700 °C, and (c) reaction rate constant (k) of the samples.

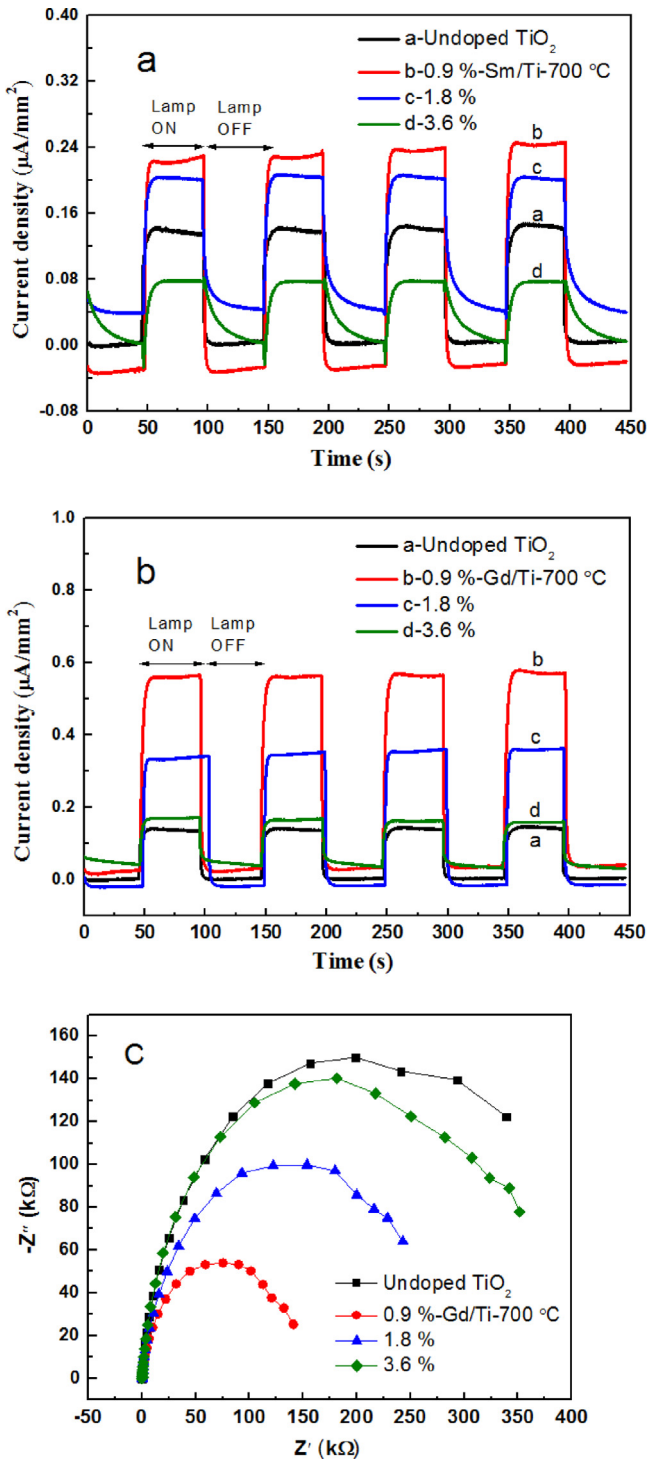

Fig. 9. Photocurrent response of undoped, 0.9, 1.8 and 3.6 at.% Sm-TiO_2 (a), Gd-TiO_2 nanocomposites sintered at 700 °C under irradiation of simulated solar light without any bias potential (b) and EIS Nyquist plots of undoped, 0.9, 1.8 and 3.6 at.% Gd-TiO_2 nanocomposite sintered at 700 °C (c).

the photocurrent intensity increases by increasing the amount of Sm and Gd dopants up to 0.9 at.% afterwards decreases by further increase of their amounts. This could be an evidence of increasing the recombination of photogenerated electron-hole pairs for doped samples at 1.8 and 3.6 at%. It is to be mentioned that by increasing the amount of dopant the average particle size of the nanocomposite samples decrease (Fig. 7) and so the effective surface area increase which can increase the surface defects and surface recom-

bination rate. It was found that the photocurrent responses of the samples were highly reproducible and remain stable for several on/off cycles, indicating an effective stability against photocorrosion. These observations were well confirmed by PL results.

In order to understand the electron transfer properties better, EIS measurements was performed for the corresponding photoanodes of Gd-doped TiO_2 nanocomposite sintered at 700 °C. The results are represented in Fig. 9c. It can be seen that the 0.9 at.% Gd-doped TiO_2 composite nanoparticles shows smallest semicircle at high frequencies, indicating the more efficient separation and transfer efficiency of photogenerated electron-hole pairs which is compatible with its highest photocurrent response (Fig. 9b). It is to be noticed that although the photocurrent is a maximum for 0.9 at.% for the doped samples but the photo degradation of Congo red dye is maximum for 1.8 at.% doped samples (Fig. 8c) which means other factors such as crystallinity, adsorption of the dye's molecules to the photocatalyst nanoparticles and diffusion of light due to the porosity of the samples are essential in improvement of photocatalytic performance.

4. Conclusion

Undoped TiO_2 and Sm or Gd/TiO_2 composite nanoparticles in different molar ratios were prepared through the combined sol–gel milling method. Congo red dye adsorption and photocatalytic properties of samples were measured. Sample's characterizations revealed high temperature anatase stability of undoped samples up to 700 °C and of composite samples even beyond 700 °C that led to high photocatalytic performance without presence of rutile phase. It was found that the particle size was decreased by doping and almost narrow size distribution of the composite particles enhanced their dye adsorption and photodegradation performance. The results showed that the Gd-doped samples had higher crystallinity and porosity compared to the Sm-doped samples. The photocurrent results showed that the TiO_2 nanocomposite samples response to the light better which means that the nanocomposite samples have stronger ability to produce charge carriers and participate in the photocatalytic reactions. Also the dye photodegradation performance of the samples with 1.8 at.% of dopant was a maximum for both Sm and Gd/TiO_2 composite nanoparticles. The decrease in photocatalytic performance of the samples with 3.6% of dopant was ascribed to the increase in the surface recombination of electron-hole pairs due to increase in the specific surface area. We believe that the surface modification of TiO_2 nanoparticles by Sm or Gd doping is responsible for the different behaviors of these nanocomposites and the Gd/TiO_2 performance was much more effective than that of the Sm/TiO_2.

Acknowledgment

The authors acknowledge Shahid-Chamran university of Ahvaz for the financial support of this work.

References

[1] A.Z. Moshfegh, Nanoparticle catalysts, J. Phys. D: Appl. Phys. 42 (2009) 233001–233031.
[2] R. Leary, A. Westwood, Carbonaceous nanomaterials for the enhancement of TiO_2 photocatalysis, Carbon 49 (2011) 741–772.
[3] Ch.M. Teh, A.R. Mohamed, Roles of titanium dioxide and ion-doped titanium dioxide on photocatalytic degradation of organic pollutants (phenolic compounds and dyes) in aqueous solutions: a review, J. Alloy Compd. 509 (2011) 1648–1660.
[4] L. Ren, Y. Li, J. Hou, X. Zhao, Ch. Pan, Preparation and enhanced photocatalytic activity of TiO_2 nanocrystals with internal pores, ACS Appl. Mater. Interfaces 6 (2014) 1608.
[5] K. Naeem, F. Ouyang, Preparation of Fe^{3+}-doped TiO_2 nanoparticles and its photocatalytic activity under UV light, Phys. B 405 (2010) 221–226.
[6] N.L.V. Carreno, I.T.S. Garcia, L.S.S.M. Carreno, M.R. Nunes, Synthesis of titania/carbon nanocomposites by polymeric precursor method, J. Phys. Chem. Sol. 69 (2008) 1897–1904.
[7] J. Zou, B. Zhu, L. Wang, X. Zhang, Zh. Mi, Zn- and La-modified TiO_2 photocatalysts for the isomerization of norbornadiene to quadricyclane, J. Mol. Catal. A-Chem. 286 (2008) 63–69.
[8] M. Crişan, N. Dragan, D. Crisan, A. Ianculescu, I. Nitoi, P. Oancea, L. Todan, C. Stan, N. Stănică, The effects of Fe, Co and Ni dopants on TiO_2 structure of sol–gel nanopowders used as photocatalysts for environmental protection: a comparative study, Ceram. Int. 42 (2016) 3088–3095.
[9] Y. Liu, J. Liu, Y. Lin, Y. Zhang, Y. Wei, Simple fabrication and photocatalytic activity of S-doped TiO_2 under low power LED visible light irradiation, Ceram. Int. 35 (2009) 3061–3065.
[10] L. Zhou, J. Deng, Y. Zhao, W. Liu, L. An, F. Chen, Preparation and characterization of N–I co-doped nanocrystal anatase TiO_2 with enhanced photocatalytic activity under visible-light irradiation, Mater. Chem. Phys. 117 (2009) 522–527.
[11] J.A. Rengifo-Herrera, C. Pulgarin, Photocatalytic activity of N, S co-doped and N-doped commercial anatase TiO_2 powders towards phenol oxidation and E. coli inactivation under simulated solar light irradiation, Sol. Energy 84 (2010) 37–43.
[12] M. Pelaez, A.A. de la Cruz, E. Stathatos, P. Falaras, D.D. Dionysiou, Visible light-activated N-F-codoped TiO_2 nanoparticles for the photocatalytic degradation of microcystin-LR in water, Catal. Today 144 (2009) 19–25.
[13] T. Jiang, L. Zhang, M. Ji, Q. Wang, Q. Zhao, X. Fu, H. Yin, Carbon nanotubes/TiO_2 nanotubes composite photocatalysts for efficient degradation of methyl orange dye, Particuology 11 (2013) 737–742.
[14] K. Dai, X. Zhang, K. Fan, T. Peng, B. Wei, Hydrothermal synthesis of single-walled carbon nanotube–TiO_2 hybrid and its photocatalytic activity, Appl. Surf. Sci. 270 (2013) 238–244.
[15] Y. Zhang, Z. Zhou, T. Chen, H. Wang, W. Lu, Graphene TiO_2 nanocomposites with high photocatalytic activity for the degradation of sodium pentachlorophenol, J. Environ. Sci. 26 (2014) 2114–2122.
[16] X. Pan, Y. Zhao, Sh. Liu, C.L. Korzeniewski, Sh. Wang, Zh. Fan, Comparing Graphene-TiO_2 nanowire and Graphene-TiO_2 nanoparticle composite photocatalysts, ACS Appl. Mater. Interfaces 4 (2012) 3944–3950.
[17] W. Han, Ch. Zang, Z. Huang, H. Zhang, L. Ren, X. Qi, J. Zhong, Enhanced photocatalytic activities of three-dimensional graphene-based aerogel embedding TiO_2 nanoparticles and loading MoS_2 nanosheets as Co-catalyst Int, J. Hydrogen Energy 39 (2014) 19502–19512.
[18] Y. Ao, J. Xu, D. Fu, Ch. Yuan, Preparation of Ag-doped mesoporous titania and its enhanced photocatalytic activity under UV light irradiation, J. Phys. Chem. Sol. 69 (2008) 2660–2664.
[19] M. Huang, Ch. Xu, Z. Wu, Y. Huang, J. Lin, J. Wu, Photocatalytic discolorization of methyl orange solution by Pt modified TiO_2 loaded on natural zeolite, Dyes Pigm. 77 (2008) 327–334.
[20] J. Yu, L. Yue, Sh. Liu, B. Huang, X. Zhang, Hydrothermal preparation and photocatalytic activity of mesoporous Au–TiO_2 nanocomposite microspheres, J. Colloid Interface Sci. 334 (2009) 58–64.
[21] N. Venkatachalam, M. Palanichamy, V. Murugesan, Sol–gel preparation and characterization of alkaline earth metal doped nano TiO_2: efficient photocatalytic degradation of 4-chlorophenol, J. Mol. Catal. A- Chem. 273 (2007) 177–185.
[22] X. Li, R. Xiong, G. Wei, Preparation and photocatalytic activity of nanoglued Sn-doped TiO_2, J. Hazard. Mater. 164 (2009) 587–591.
[23] R. Yuan, B. Zhou, D. Hua, Ch. Shi, Enhanced photocatalytic degradation of humic acids using Al and Fe co-doped TiO_2 nanotubes under UV/ozonation for drinking water purification, J. Hazard. Mater. 262 (2013) 527–538.
[24] Q. Chen, D. Jiang, W. Shi, D. Wu, Y. Xu, Visible-light-activated Ce–Si co-doped TiO_2 photocatalyst, Appl. Surf. Sci. 255 (2009) 7918–7924.
[25] M. Farbod, M. Kajbafvala, Effect of nanoparticle surface modification on the adsorption-enhanced photocatalysis of Gd/TiO_2 nanocomposite, Powder Technol. 239 (2013) 434–440.
[26] T. Liu, X. Li, F. Li, Enhanced photocatalytic activity of Ce^{3+}-TiO_2 hydrosols in aqueous and gaseous phases, Chem. Eng. J. 157 (2010) 475–482.
[27] J. Shi, J. Zheng, P. Wu, Preparation, characterization and photocatalytic activities of holmium-doped titanium dioxide nanoparticles, J. Hazard. Mater. 161 (2009) 416–422.
[28] J. Liqiang, S. Xiaojun, X. Baifu, W. Baiqi, C. Weimin, F. Honggang, The preparation and characterization of La doped TiO_2 nanoparticles and their photocatalytic activity, J. Solid State Chem. 177 (2004) 3375–3382.
[29] Y. Xie, Ch. Yuan, Photocatalysis of neodymium ion modified TiO_2 sol under visible light irradiation, Appl. Surf. Sci. 221 (2004) 17–24.
[30] Ch. Liang, F. Li, Ch. Liu, J. Lu, X. Wang, The enhancement of adsorption and photocatalytic activity of rare earth ions doped TiO_2 for the degradation of Orange I, Dyes Pigm. 76 (2008) 477–484.
[31] Q. Xiao, Zh. Si, J. Zhang, Ch. Xiao, X. Tan, Photoinduced hydroxyl radical and photocatalytic activity of samarium-doped TiO_2 nanocrystalline, J. Hazard. Mater. 150 (2008) 62–67.
[32] D.G. Huang, S.J. Liao, W.B. Zhou, S.Q. Quan, L. Liu, Z.J. He, J.B. Wan, Synthesis of samarium- and nitrogen-co-doped TiO_2 by modified hydrothermal method and its photocatalytic performance for the degradation of 4-chlorophenol, J. Phys. Chem. Solids 70 (2009) 853–859.
[33] J. Xu, Y. Ao, D. Fu, Ch. Yuan, Synthesis of Gd-doped TiO_2 nanoparticles under mild condition and their photocatalytic activity, Colloids Surf. A 334 (2009) 107–111.

[34] M. Saif, M.S.A. Abdel-Mottaleb, Titanium dioxide nanomaterial doped with trivalent lanthanide ions of Tb, Eu and Sm: preparation, characterization and potential applications, Inorg. Chim. Acta 360 (2007) 2863–2874.
[35] H. Liu, L. Yu, W. Chen, Y. Li, The progress of TiO_2 nanocrystals doped with rare earth ions, J. Nanomater. 2012 (2012), article ID 235879, 9 pages.
[36] M. Zalas, Gadolinium-modified titanium oxide materials for photoenergy applications: a review, J. Rare Earth 32 (2014) 487–495.
[37] N. Qin, J. Xiong, R. Liang, Y. Liu, Sh. Zhang, Y. Li, Zh. Li, L. Wu, Highly efficient photocatalytic H_2 evolution over MoS_2 nanofibers prepared by an electrospinning mediated photodeposition method, Appl. Catal. B-Environ. 202 (2017) 374–380.
[38] D.P. Kumar, S. Hong, D.A. Reddy, T.K. Kim, Ultrathin MoS_2 layers anchored exfoliated reduced graphene oxide nanosheet hybrid as a highly efficient co catalyst for CdS nanorods towards enhanced photocatalytic hydrogen production, Appl. Catal. B-Environ. 212 (2017) 7–14.
[39] Ch. Liu, L. Wang, Y. Tang, Sh. Luo, Y. Liu, Sh. Zhang, Y. Zeng, Y. Xu, Vertical single or few-layer MoS_2 nanosheets rooting into TiO_2 nanofibers for highly efficient photocatalytic hydrogen evolution, Appl. Catal. B-Environ. 164 (2015) 1–9.
[40] Q. Zhang, Y. Huang, Sh. Peng, Y. Zhang, Zh. Shen, J.-j. Cao, W. Ho, Sh. Ch. Lee, D.Y.H. Pui, Perovskite $LaFeO_3$-SrTiO composite for synergistically enhanced NO removal under visible light excitation, Appl. Catal. B-Environ. 204 (2017) 346–357.
[41] Zh. Wang, Y. Huang, W. Ho, J. Cao, Zh. Shen, Sh.Ch. Lee, fabrication of $Bi_2O_2CO_3$/g-C_3N_3 heterojunctions for efficiently photocatalytic NO in air removal: *In-Situ* self-Sacrificial synthesis, characterizations and mechanistic study, Appl. Catal. B-Environ. 199 (2016) 123–133.